

Supporting Information

Integrated sampling-and-sensing using microdialysis and Biosensing by Particle Motion for continuous cortisol monitoring

Laura van Smeden^{a,c}, Arthur M. de Jong^{b,c}, and Menno W. J. Prins^{*a,b,c,d}

^aDepartment of Biomedical Engineering, Eindhoven University of Technology, 5600 MB Eindhoven, The Netherlands.

^bDepartment of Applied Physics, Eindhoven University of Technology, 5600 MB Eindhoven, The Netherlands.

^cInstitute for Complex Molecular Systems (ICMS), Eindhoven University of Technology, 5600 MB Eindhoven, The Netherlands.

^dHelia Biomonitoring, De Lismortel 31, 5612 AR Eindhoven, The Netherlands.

*email: m.w.j.prins@tue.nl

Contents

1	Cortisol detection using UV-vis spectroscopy	2
2	Droplet evaporation during sample collection	3
3	Membrane permeability	5
4	Osmotic pressure in microdialysis under influence of albumin protein	6
5	Dialysis versus retro-dialysis for medium with albumin	7
6	Azorubine detection using optical microscopy	8
7	Influence of membrane length on sampling of azorubine	9
8	Dimensions of flow cell	11
9	Continuous cortisol monitoring with BPM	12
10	Supporting Tables	15
11	References	17

1 Cortisol detection using UV-vis spectroscopy

The cortisol concentration in PBS was quantified by UV-vis spectroscopy by measuring the absorbance peak at 247 nm (Fig. S1A). An individual calibration curve was established per experiment by a 3-times dilution series ranging from 600 μM to 2.5 μM cortisol. The four examples in Fig. S1B demonstrate the linearity over the tested concentration range and a limit of detection of 3.9 ± 2.6 μM based on four calibrations (obtained via $\mu + 3 \cdot \sigma$ of the absorbance, with μ the average of the blank measured in triplicate, and with σ the standard deviation of the blanks).

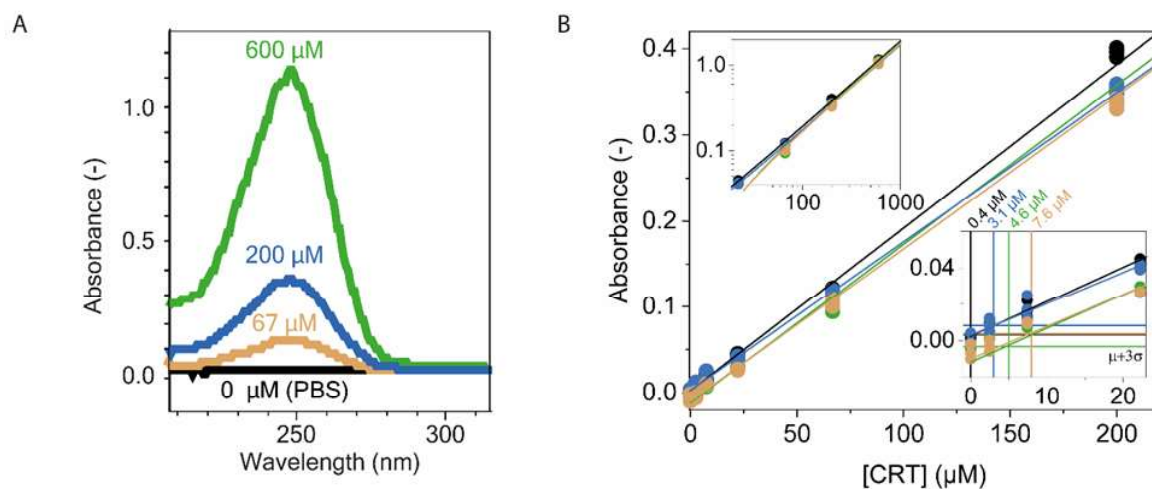


Figure S1: Cortisol detection via absorbance at 247 nm. A) Cortisol absorbance spectra for three cortisol concentrations. B) Four examples of cortisol calibration curves for absorbance at 247 nm obtained via UV-vis spectroscopy. Top inset shows calibration curves with logarithmic scales highlighting the total measurement range. Bottom inset shows a zoom-in for the lower concentrations with the horizontal lines indicating the $\mu+3\sigma$ of the absorbance of the blank. The vertical lines indicate the limits of detection calculated from the four calibration curves using $\mu+3\sigma$ (0.4 μM for black, 3.1 μM for blue, 4.6 μM for green, and 7.6 μM for brown). From the four values, the averaged LoD is determined to be 3.9 ± 2.6 μM .

2 Droplet evaporation during sample collection

UV-vis spectroscopy measurements on a Nanodrop instrument require a minimum sample volume of 2 μl , but for reliable pipetting and transfer of the sample, a total sample volume of about 10 μl is required per measurement. Samples were collected from the outlet of a microdialysis catheter. Every sample was collected as a single droplet that forms at the end of the microdialysis outlet tubing, which was forced to fall into a collection vial with a capacity of about 200 μl , after which the vial was immediately closed.

The time required to perfuse a volume of 10 μl depends on the flowrate of the perfusion pump. Perfusion of 10 μl with a flowrate of 2 $\mu\text{l}/\text{min}$ takes 5 min, and with a flowrate of 0.5 $\mu\text{l}/\text{min}$ it takes 20 min. During this time partial evaporation takes place of the droplet that hangs at the end of the microdialysis outlet tubing. The water evaporation increases the analyte concentration in the collected fluid and is most important for low flow rates, due to the longer time that is needed for perfusing a 10 μl volume.

The consequences of droplet evaporation are shown in Fig. S2. The green datapoints in Fig. S2A represent a control experiment with fluid droplets sitting on a flat substrate. 10 μl droplets located on a flat substrate show a linear decrease of weight as a function of time, with a loss rate of ~ 0.2 mg/min due to evaporation, so a volume loss rate of ~ 0.2 $\mu\text{l}/\text{min}$, illustrating the significance of the evaporation process.

The microdialysis datapoints in Fig. S2A show the sample weight that was collected from the microdialysis outlet tubing. The microdialysis catheter was perfused with three different flowrates: 2 $\mu\text{l}/\text{min}$ (black), 1 $\mu\text{l}/\text{min}$ (blue), and 0.5 $\mu\text{l}/\text{min}$ (pink). The data show that a lower flowrate with longer sampling time, results in a lower collected sample weight. All sample weights are slightly above 10 mg, which may have been caused by a systematic deviation in the weight measurement or in the fluidic system. The observed mass decrease as a function of collection time shows a loss rate of 0.089 ± 0.046 mg/min (fitted straight line), which is attributed to droplet evaporation. Evaporation losses were also calculated according to $R_{\text{evaporation}} = C \cdot A \cdot x_{\text{max}}(1 - H)$, with $R_{\text{evaporation}}$ the evaporation rate (kg/h), C the evaporation constant of 25 kg/m²h (assuming a temperature of 25 °C and zero air flow), A the surface area of the droplet (m²), x_{max} the maximum saturation humidity ratio in air of 0.0198 kg/kg (kg H₂O in kg dry air at 25 °C), and H the relative humidity of 0.50 (50%). The calculations give an approximated loss rate during sample collection of 0.05 $\mu\text{l}/\text{min}$.

The cortisol concentrations were mathematically corrected with factors 89.9%, 95.0% and 97.7% applied for the flowrates of 0.5, 1, and 2 $\mu\text{l}/\text{min}$, respectively. With these corrections, the measured cortisol concentrations and recoveries are reduced with respect to the Nanodrop measurements, see Fig. S2B. At the lowest flow speed, the uncorrected recovery is larger than 100%, and the corrected recovery is around 100% ($96 \pm 1\%$ based on multiple experiments; see Fig. 2). Compared with the cortisol recovery reported by Schuck in 2004 ($53.5 \pm 9.6\%$ for a 2 $\mu\text{l}/\text{min}$ flowrate with a 10 mm membrane of a CMA/20 probe with 20 kDa MWCO)¹, this corresponds with a permeability coefficient of 1.2-2.1 $\mu\text{m}/\text{s}$, which agrees with the permeability coefficient of 1.2 $\mu\text{m}/\text{s}$ as determined based on the data of Fig. 2B.

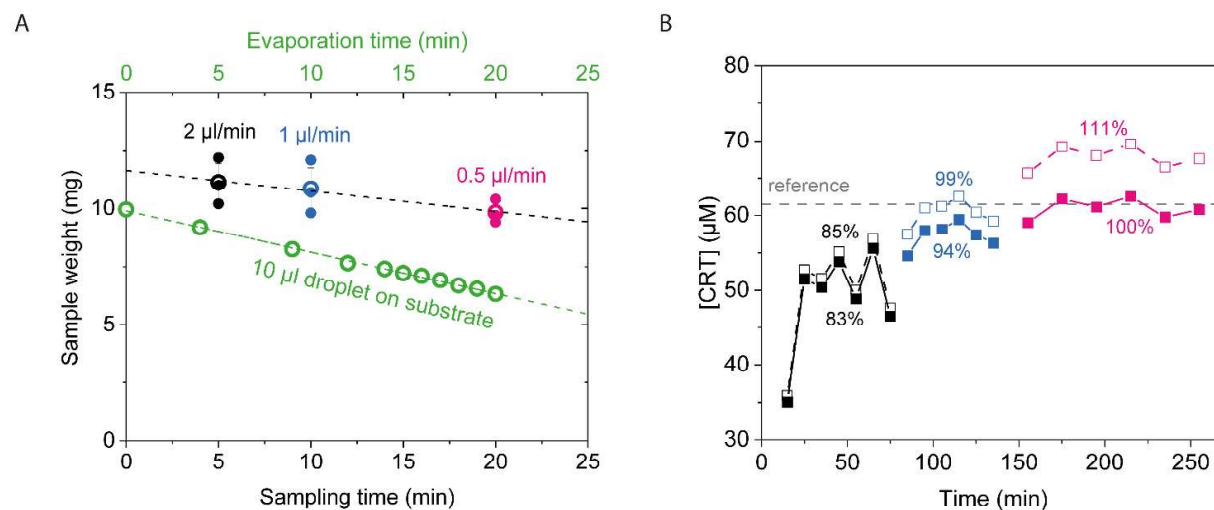


Figure S2: Evaporation of water droplets during dialysate collection. A) Collected sample weight for three different flow rates and corresponding sampling times. The times were set for a total pump infusion volume of 10 µl. Flowrates were 0.5 (pink), 1 (blue), and 2 (black) µl/min. Filled circles show the measured weight and the open circles present the average weight with error bars based on n=3. Black dashed line is a linear fit with a slope of -0.089 ± 0.046 mg/min. The green data indicates the weight of a 10 µl droplet on a substrate and how the weight decreased over time via evaporation. The green dashed line is a linear fit with a slope of -0.18 mg/min. B) Effect of applying corrections on the detected cortisol concentrations. Open symbols represent the uncorrected recovery and closed symbols represent the recovery with evaporation correction.

3 Membrane permeability

The semi-permeable membrane of the microdialysis probe functions as a physical barrier to separate large proteins and cells from the perfusate while molecules below a given molecular weight cut-off (MWCO) should be able to reach the dialysate. The size selectivity of the used microdialysis probes with 4 mm and 30 mm membrane lengths was studied using SDS-PAGE by analysing the protein content of dialysate obtained from PBS, PBS with albumin (BSA), porcine plasma, and whole porcine blood (Fig. S3). The SDS-PAGE protein gel has a protein content limit of detection of 0.8 µg/ml (specified by supplier), and as there are no detectable bands, the dialysate of both the 4 mm and 30 mm probe contain less than 0.8 µg/ml protein per protein moiety. The gel shows clear bands around ~55 kDa (apparent molecular weight), representing BSA (66 kDa) and albumin from porcine blood plasma. Porcine blood plasma also contains proteins with a higher molecular weight, being ~68 kDa (possibly fibrinogen chains²), 250 kDa, and a protein larger than 250 kDa. Comparing the undiluted dialysate with the 80× diluted 40% BSA sample and the 320× diluted plasma sample, the microdialysis membrane results in an efficient separation of proteins from the perfusate and dialysate.

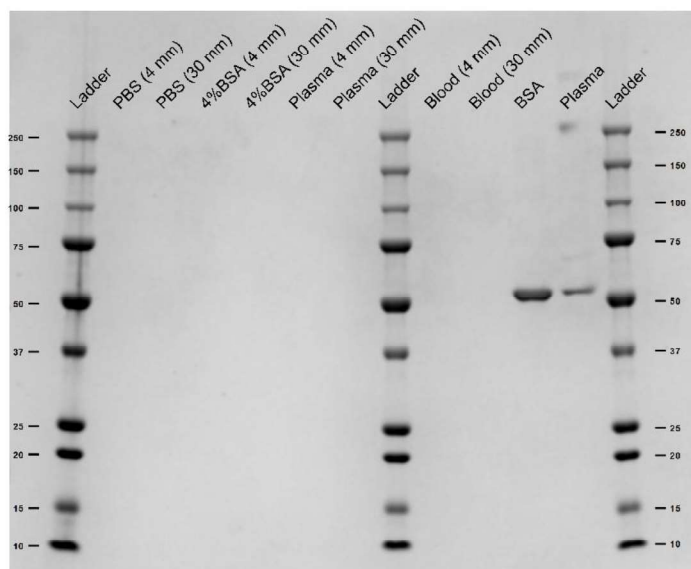


Figure S3: Microdialysis membrane permeability. SDS-PAGE gel with dialysate obtained from PBS, 4% BSA, plasma, and whole blood. Protein bands are absent in the dialysate samples, meaning that there is less than 0.8 µg/ml protein. The loaded protein content of BSA and plasma is 0.2 mg/ml, obtained via 80× and 320× dilution, respectively.

4 Osmotic pressure in microdialysis under influence of albumin protein

Microdialysis is based on diffusive transport of analyte across a semi-permeable membrane. Besides analyte, other molecules with molecular weights below the molecular weight cut-off (MWCO) of 20 kDa, can also pass the membrane. Large molecules, such as albumin (~66 kDa) remain in their compartment, but can be a driving force for osmotic pressure, leading to transport of water molecules. This effect is visualized in Fig. S4A, where a decrease in collected sample weight is visible for 40% BSA samples (43-98%) and partially for 4% BSA (16-24%) compared to PBS. Osmotic pressure effects can be limited using macromolecules like Dextran in the perfusate³, which will be interesting for follow-up research in case sampling from media with high protein content is studied.

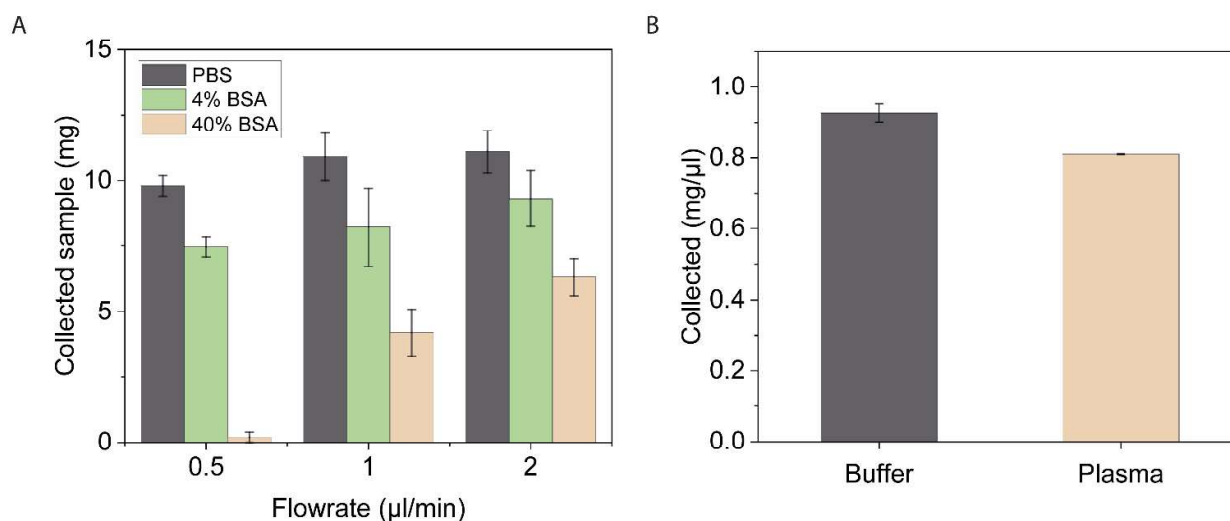


Figure S4: Dialysate collection from different media, for a microdialysis probe with a membrane length of 30 mm and PBS as perfusate. A) Collected sample weight for different flowrates, for sampling 10 µl from PBS (grey), 4% BSA in PBS (green), and 40% BSA in PBS (brown). B) Collected sample weight per added perfusate volume at a flowrate of 2 µl/min, collected in vials at the waste of a system with microdialysis probe coupled to a BPM sensor flow cell (see Fig. 5A). The data for buffer (PBS with 0.5 M NaCl and 0, 5, or 20 µM cortisol) is based on 6 samples where ~80 µl perfusate was added and the data for plasma (human blood plasma with 0.5 M NaCl and 21 µM cortisol) is based on ~1.5 ml perfusate addition.

5 Dialysis versus retro-dialysis for medium with albumin

For microdialysis sampling from 4% BSA, a lower recovery is observed in a dialysis experiment compared to a retro-dialysis experiment, see Figs. S5A and S5B. We attribute the lower recovery in the dialysis experiment to a reduced free cortisol concentration, as cortisol binds with an estimated binding affinity of 0.33 mM to albumin and with an estimated binding affinity of 23 nM to corticosteroid-binding globulin (CBG)⁴. In whole blood with 10 μM as total cortisol concentration (free plus bound), these binding affinities cause $\sim 50\%$ of cortisol to bind to albumin (present at a concentration of ~ 0.6 mM) and almost saturated binding to CBG (present at a concentration of 0.65 μM , so corresponding to $\sim 6\%$ of the total cortisol concentration)^{4,5}. Within a period of 30 min (Fig. S3A), the recovery from 4% BSA reached a plateau of $\sim 79\%$ at 0.5 $\mu\text{l}/\text{min}$. This indicates that $\sim 17\%$ cortisol is bound to albumin (only free cortisol can pass through the 20 kDa semi-permeable membrane), as a recovery of $\sim 96\%$ is expected based on the data obtained via retro-dialysis (Fig. S5BC). This decrease in free cortisol concentration will be further investigated in follow-up research.

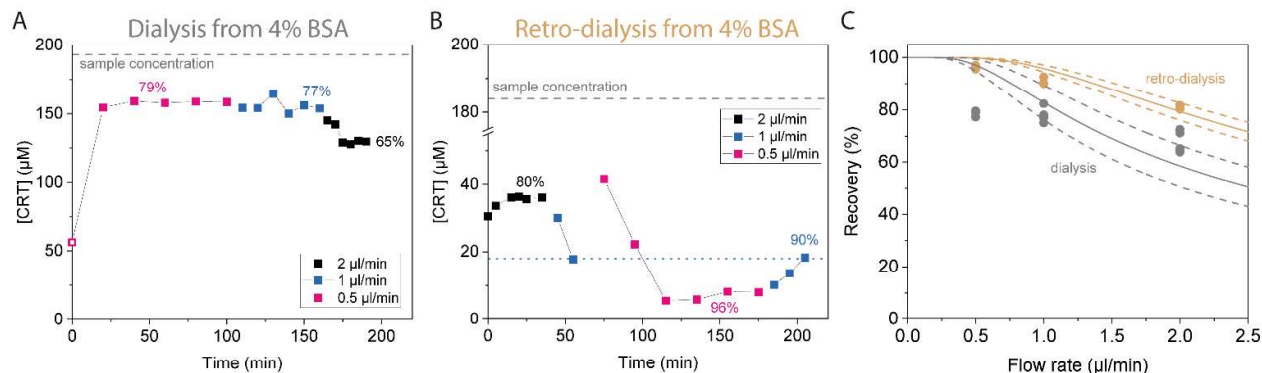


Figure S5: Microdialysis sampling from 4% BSA with a 30 mm membrane length. A) Cortisol concentration of dialysate obtained by sampling from 4% BSA spiked with ~ 195 μM cortisol, with PBS as perfusate. The cortisol spike was applied directly before the start of the measurement (5–10 min before the first datapoint). B) Cortisol concentration of retro-dialysis obtained by sampling from 4% BSA, with as perfusate PBS with ~ 185 μM cortisol. C) Recovery comparison for dialysis (grey, data from panel A) and retro-dialysis (brown, data from panel B).

6 Azorubine detection using optical microscopy

Investigation of the integration of microdialysis with a flow cell was done using azorubine, a red food colorant of 502 Da. Azorubine strongly absorbs light, already visible by eye. To quantify the azorubine concentration, a bright field microscope setup was used in combination with a 510 nm bandpass filter, as visualized in the bottom left panel of Fig. 1. The light intensity as observed with microscopy were used to calculate [azo] using the Law of Lambert Beer ($\frac{I_x}{I_0} = 10^{-E} = 10^{-\epsilon \cdot [azo] \cdot d}$)⁶, with I_0 the maximum intensity observed in the flow cell in the absence of azorubine, I_x the detected intensity, ϵ the absorption of azorubine at 510 nm ($24000 \text{ M}^{-1}\text{cm}^{-1}$)⁷, and d the thickness of the measurement chamber in the flow cell (0.45 mm). Fig. S6 shows the detection of the calibration samples (panel A), the exponential relation between the azorubine concentration and the normalized light intensity (panel B), and the calculated azorubine concentration (panel C).

Calibration measurements were done (without the microdialysis probe), with a flowrate of $100 \mu\text{l}/\text{min}$ and $200 \mu\text{l}$ per concentration step, see Fig. S6A. After roughly 30 s of flow, the intensity changes because of the arrival of the calibration sample in the flow cell chamber. After 2 min, the flow cell chamber is completely filled with the calibration sample, and the intensity corresponding with the calibration sample concentration was determined. Fig S6B shows the normalized steady-state intensities ($\frac{I_x}{I_0}$ based on panel A; logarithmic scale) as a function of the azorubine stock dilution (linear scale). The datapoints were fitted with an exponential function: $\frac{I_x}{I_0} = 10^{-\epsilon \cdot [azo]_{\text{stock}} \cdot f_{\text{dilution}} \cdot d}$, which corresponds with $\epsilon=24000 \text{ M}^{-1}\text{cm}^{-1}$, $d=0.45 \text{ mm}$, and an azorubine stock concentration [azo]_{stock} of $47 \pm 3 \text{ mM}$. The azorubine dilution of 0.02 (pink line in panel A) is at the 95% confidence interval of the fit in panel B. The stock dilution of 0.04 (grey line in panel A) deviates from the exponential fit in panel B because the absolute intensity (panel A) is close to zero, leading to systematic errors. Fig. S6C shows the calculated azorubine concentrations over time. The concentration-time profiles show an average total delay time of $\Delta t_{95\%} = t_0 + 3\tau = 95 \pm 11 \text{ s}$. This relates to a flowrate of $100 \mu\text{l}/\text{min}$ and a tubing volume of $\sim 59 \mu\text{l}$ and means that 2 min of flow was sufficient to reach steady-state signals for calibration of the azorubine concentration using optical microscopy.

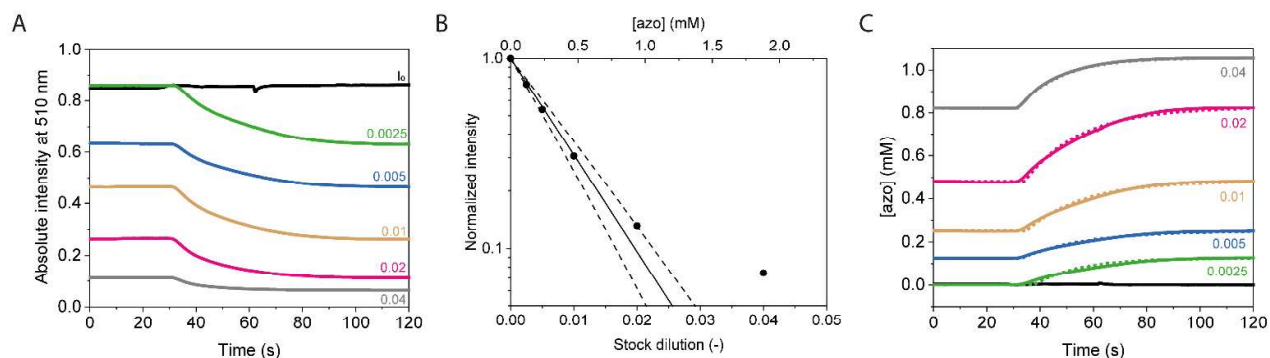


Figure S6: Methodology to quantify azorubine concentration as a function of time. A) Absolute light intensity at 510 nm as observed in the complete FOV of the $12 \mu\text{l}$ flow cell during a 2-minute addition of azorubine using a flowrate of $100 \mu\text{l}/\text{min}$ and an approximately 13 cm long flexible tubing with an inner diameter of 0.76 mm ($\sim 59 \mu\text{l}$). Curve labels show the azorubine stock dilution factor used in the experiment. B) Normalized steady-state intensities (logarithmic scale) as a function of azorubine stock dilution. Dots are based on the steady-state values of panel A. The line is an exponential fit with a slope corresponding with an azorubine stock concentration of $47 \pm 3 \text{ mM}$, based on $\epsilon=24000 \text{ M}^{-1}\text{cm}^{-1}$ and $d=0.45 \text{ mm}$. Dashed lines indicate the 95% confidence interval of the exponential fit. C) Azorubine concentration as observed in the flow cell, calculated using the data of panel A and the Law of Lambert Beer. Dotted lines represent fitted curves, with a delay time of $35 \pm 2 \text{ s}$ and an exponential relaxation with a τ -value of $20 \pm 3 \text{ s}$ (see Table S6).

7 Influence of membrane length on sampling of azorubine

As was demonstrated in Fig. 2B for cortisol sampling with microdialysis, a shorter membrane length results in a lower recovery. This section focusses on the sampling-and-sensing of azorubine with a microdialysis probe with a 4 mm membrane length (left side of Fig. S7) in comparison with a 30 mm membrane length (right side of Fig. S7, same data as Fig. 4A and Fig. 4B). Here, the influence of the membrane length on the azorubine recovery is investigated, the azorubine permeability coefficient is determined, and the concentration-time profiles are analysed.

The 4 mm membrane (Fig. S7A) has an azorubine recovery of ~25%, and the 30 mm membrane (Fig. S7B) a recovery of ~65%. The recovery for the 30 mm membrane length is expected to be an underestimation, as concentration determinations for higher concentrations (>0.60 mM) are less accurate (see Fig. S6). Therefore, a recovery of $88 \pm 4\%$ that is based sampling from a range of azorubine concentrations (demonstrated in the inset of Fig. 4A), is probably more representative for the 30 mm membrane. Based on the azorubine recovery, flowrate, and membrane area, a permeability coefficient of $\sim 1.4 \mu\text{m/s}$ was determined, which is in the same order of magnitude as cortisol ($\sim 1.2 \mu\text{m/s}$) and glucose ($\sim 0.9 \mu\text{m/s}$ at 26°C and $\sim 1.0 \mu\text{m/s}$ at 37°C)⁸. The similar permeability coefficient and recovery values of azorubine and cortisol (30 mm membrane: azorubine recovery of $83 \pm 4\%$ and cortisol recovery of 55-85%), indicate that the molecules of respectively 502 Da and 362 Da can easily pass through the 20-kDa MWCO of the semi-permeable membrane.

The bottom panel of Fig. S7 shows concentration-time profiles for applied step functions. The range between upper and lower azorubine concentration in dialysate decreases somewhat for subsequent cycles, possibly caused by fluid transfer between the sampling vials. Studies of the concentration-time profiles of the 4 mm membrane shows a delay time (t_0) of 3.3 ± 0.2 min and a characteristic relaxation time (τ) of 1.3 ± 0.2 min, resulting in a total delay time $\Delta t_{95\%}$ of 7.2 ± 0.8 min. This is faster than for the 30 mm membrane ($\Delta t_{95\%}$ of 10.4 ± 1.0 min) and is expected to be caused by the shorter membrane and the smaller probe outlet volume of the probe (shaft plus membrane; $2.9 \mu\text{l}$ versus $3.4 \mu\text{l}$). Therefore, a shorter microdialysis membrane length decreases the analyte recovery and gives slightly faster concentration-time profiles.

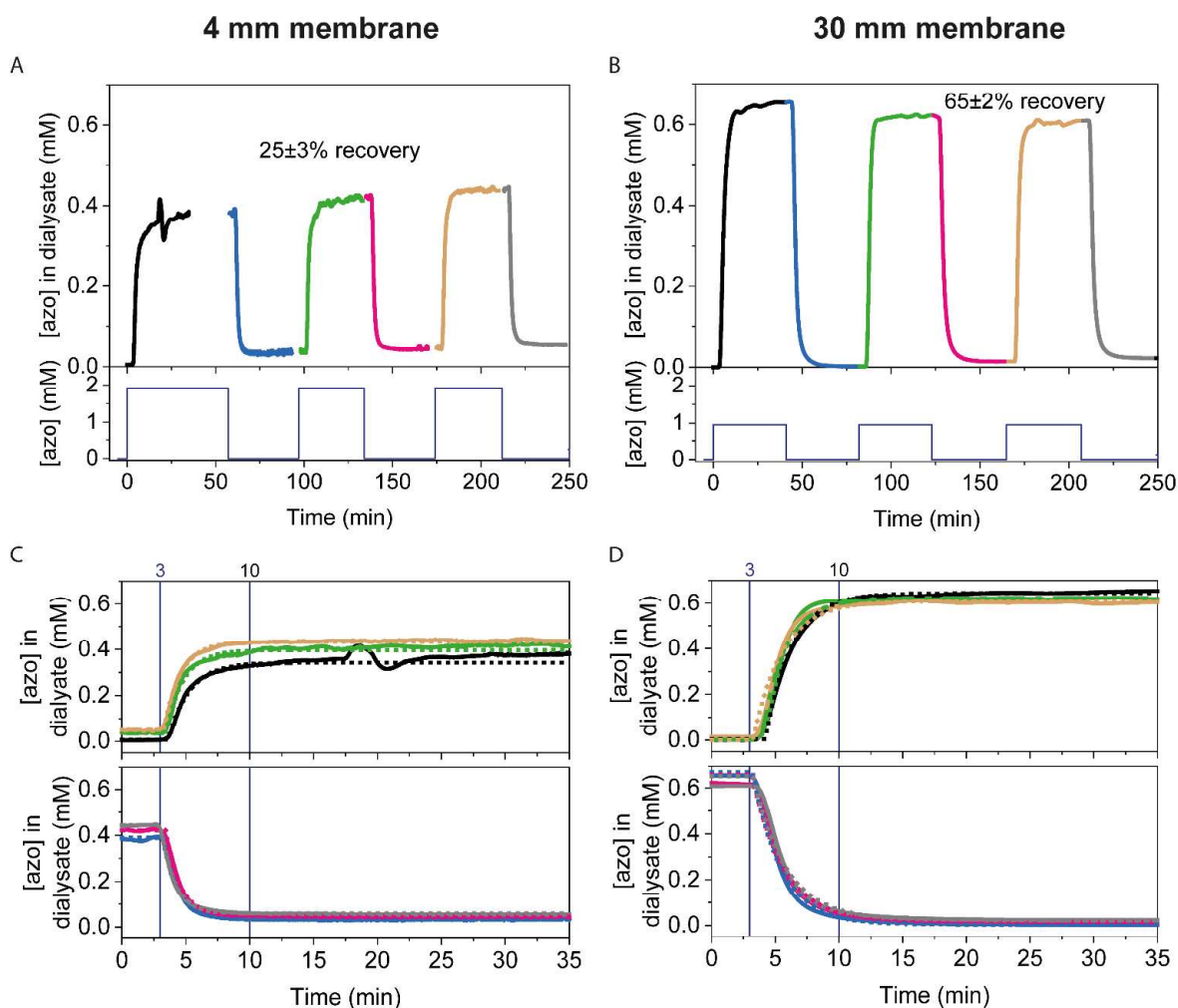


Figure S7: Time delay when sampling with microdialysis, studied with azorubine. A) Azorubine concentration in dialysate as observed for microdialysis (4 mm membrane length) connected to a flow cell, sampling from 0 up to 1.92 mM azorubine [azo], with a flowrate of 2 $\mu\text{l}/\text{min}$. B) Azorubine concentration in dialysate as observed for microdialysis (30 mm membrane length) connected to a flow cell, sampling from 0 up to 0.96 mM azorubine [azo], with a flowrate of 2 $\mu\text{l}/\text{min}$. C and D) After ~ 3.4 min (t_0 ; ~ 7 μl fluid transport corresponding with microdialysis outlet shaft + tubing) the first change of signals is detectable and after ~ 7 -10 min, fluid exchange is completed for $>95\%$ ($\Delta t_{95\%} = t_0 + \tau_{95\%}$, with $\tau_{95\%} = 3 \cdot \tau$). Dotted lines indicate the exponential fit as described in the methods and extracted values are provided in Table S3 (30 mm) and Table S7 (4 mm).

8 Dimensions of flow cell

The flow cell is based on a custom-made sticker supplied by Grace biolabs, with 4 chambers per 75x25.5 mm sticker, see Fig. S8 for more details.

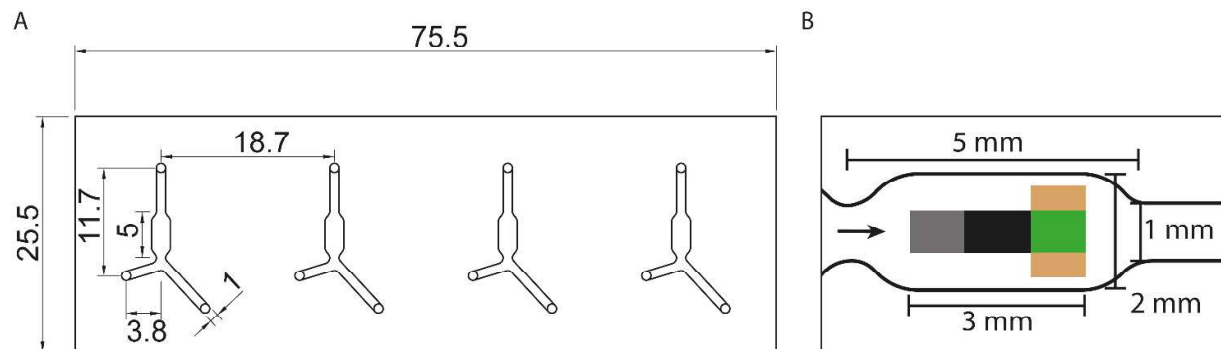


Figure S8: Dimensions of the flow cell. A) Sticker design as provided to Grace Biolabs with values indicated in mm. B) Zoom-in of the flow cell chamber. The height is 0.45 mm and the chamber has a length of 3-5 mm and a width of 1-2 mm as indicated in the image. The grey and green areas represent an area of 0.9 mm x 0.7 mm. The brown areas are each 0.9x0.4 mm. The black area in the center represents the ROI used for BPM and has an area of 1.1 mm x 0.7 mm.

9 Continuous cortisol monitoring with BPM

Fig. 5 demonstrates continuous cortisol monitoring with BPM integrated with microdialysis sampling. In this section, the BPM signal types are explained, and additional data is provided including the dose-response curves for two BPM signal types and for a repeated experiment. The reproducibility of the continuous monitoring is demonstrated, and the envisioned future application visualized.

Two BPM signal types are the bound fraction and the switching activity^{9,10}. The bound fraction is the time-averaged fraction of particle states with diffusion coefficient values below a threshold, which was selected to be $0.05 \mu\text{m}^2/\text{s}$. The switching activity indicates the (un)binding frequency of the particles per unit of time. The (un)binding of the particles with the substrate occurs because of reversible affinity-based interactions between the antibodies on the particle, the analogues on the substrate (conjugated molecules that are very similar to the analyte), and analyte, as is visualized in the bottom right panel of Fig. 1. Both BPM signal types are given in Fig. S9A and B. The signals decrease for increasing cortisol concentration, because the sensor is based on a competition assay^{9,11}. The other panels of Fig. S9 and the data of Fig. 5 show the bound fraction as BPM signal, as it can reach a higher data frequency compared with the switching activity.

The experiment presented in Fig. 5 was repeated and both data are shown in Fig. S9. The detected cortisol concentration was determined using the equation: $[\text{CRT}] = \text{EC50} \cdot \frac{S_{\text{max}} - S}{S - S_{\text{min}}}$ with S the sensor signal. S_{max} , S_{min} , and EC50 are obtained by fitting the calibration data with a sigmoidal curve: $S = S_{\text{max}} + (S_{\text{min}} - S_{\text{max}}) \cdot \frac{[\text{CRT}]}{[\text{CRT}] + \text{EC50}}$, with EC50 values of 1740 nM for Fig. 5C and Fig. S9A and 1825 nM for the data presented in Fig. S9B. The detected cortisol concentrations of both experiments are similar and show a cortisol recovery of 78-100% when sampling from buffer and 60-100% when sampling from plasma. The total time delay of both experiments is also similar with $\Delta t_{95\%} = t_0 + \tau_{95\%} = t_0 + 3\tau \cong 13 \pm 3$ min (Fig. S9D squares) compared with 13 ± 3 min (Fig. S9D circles; same data as in Fig. 5). It is also close to the total delay time as observed for azorubine monitoring ($\Delta t_{95\%}$ of 10 ± 1 min). Variations are expected to be caused by slight variations in the experimental handling, such as the start of the measurement compared to the change of sample, and the position of the FOV relative to the flow cell.

The time till the first change in the detected cortisol concentration after transferring the probe to the plasma sample (Fig. 5) showed a 2-minute longer transport time ($t_0 \sim 6$ min) compared with buffer. This is probably caused by a decrease in the flow rate in outlet tubing after the microdialysis probe because of the osmotic pressure. This is supported by the observed $\sim 22\%$ loss of dialysate compared with added perfusate, which was attributed to the osmotic pressure (see Supporting Information section 2). The effective dialysate flow rate during sampling from plasma is expected to be 1.2-1.5 $\mu\text{l}/\text{min}$, based on dividing the outlet volume (7 μl) by t_0 to correct the applied perfusate flowrate (2 $\mu\text{l}/\text{min}$).

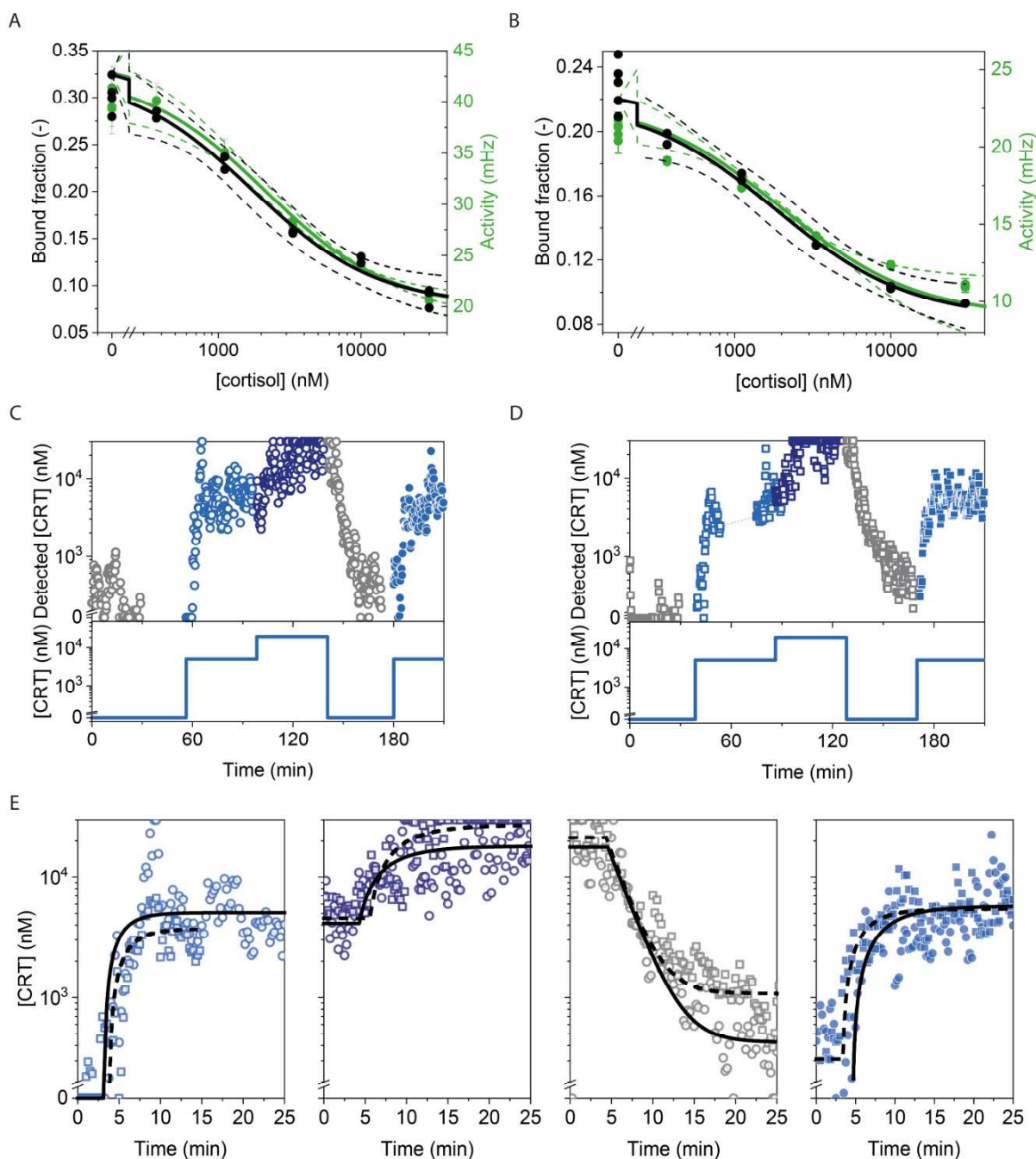


Figure S9: Demonstration of the reproducibility of cortisol monitoring via BPM and sampling with microdialysis. A) Data of the experiment in Fig. 5. Dose-response curves based on the calibration measurements performed before cortisol monitoring via BPM and sampling with microdialysis, as visualized in Fig. 5A. Data in this panel is based on the same particle motion data as in the left panel of Fig. 5C. Two BPM signal types are plotted: the left y-axis shows the bound fraction ($S_{\max} = 0.324$, $S_{\min} = 0.079$, $EC_{50} = 1740$ nM) and the right y-axis shows the switching activity. B) Dose-response curves for a reproduced microdialysis-BPM experiment with as values for the bound fraction: $S_{\max} = 0.220$, $S_{\min} = 0.083$, $EC_{50} = 1825$ nM. C) Data of the experiment in Fig. 5. Demonstration of continuous cortisol monitoring (detected [CRT]) determined based on the bound fraction sensor signal with a data frequency of 67 mHz (datapoint every 15 s). Data in this panel is based on the same particle motion data as Fig. 5, presented in Fig. 5C with a data frequency of 17 mHz. D) Repetition of the experiment as presented in panel C. Dashed blue line indicates absence of particle tracking caused by a software connection loss. E) Comparison of the data as presented in panel C (circles) and D (squares) and exponential fitting to extract delay time, of which the values are provided in Table S5 (circles; solid lines) and Table S8 (squares; dashed lines). Datapoints out of upper bounds ($>S_{\max}$) were set at zero, values were maximized till 30 μ M and values out of lower bounds ($<S_{\min}$) were removed from the dataset.

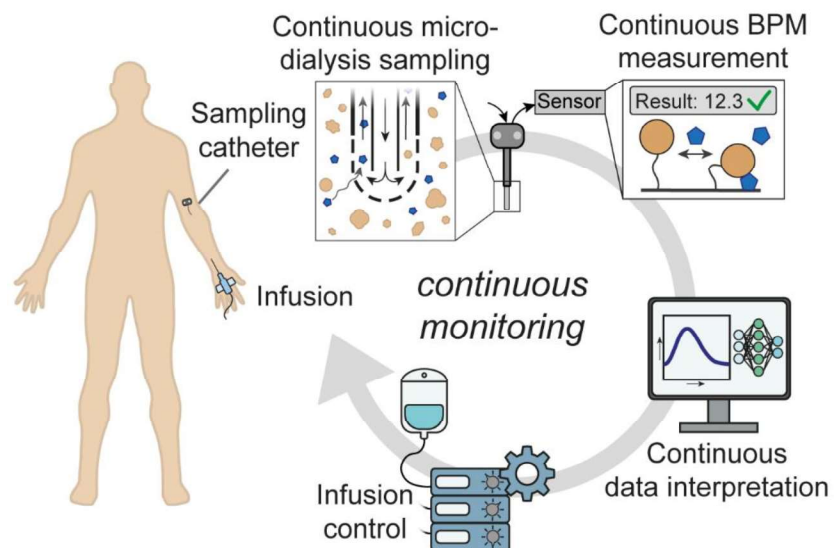


Figure S11: Schematic drawing of continuous patient monitoring in an envisioned application that combines microdialysis and BPM. Samples are obtained, measured, and analysed continuously, allowing for automated feedback loops to adjust the treatment.

10 Supporting Tables

Table S1: Fitted values of Fig. 3A. Azorubine concentration in dialysate of probe with 30 mm membrane length, for 2 $\mu\text{l}/\text{min}$ flowrate, observed for different ROIs.

Fig. 3A	Black	Gray	Green	Brown
ROIs	BPM area	Inlet side	Outlet side	Edges outlet side
t_0^* (min)	3.9	3.5	4.4	4.8
τ^* (min)	2.5	2.4	2.7	3.9

* Standard errors of the fitted t_0 -values and τ -values are smaller than 0.1 min.

Table S2: Fitted values of Fig. 3B. Normalized azorubine concentration in dialysate of probe with 30 mm membrane length, for various flowrates.

Fig. 3B	Black (2 $\mu\text{l}/\text{min}$)		Blue (1 $\mu\text{l}/\text{min}$)		Pink (0.5 $\mu\text{l}/\text{min}$)	
Concentration change	Increase	Decrease	Increase	Decrease	Increase	Decrease
t_0^* (min)	4.2	3.7	8.8	8.8	15.9	16.0
τ^* (min)	2.1	1.7	3.0	2.9	5.6	6.0
Mean t_0	4.0 min		8.8 min		16.0 min	
Mean τ	1.9 min		3.0 min		5.8 min	

*Standard errors of the fitted t_0 -values and τ -values are smaller than 0.1 min.

Table S3: Fitted values of Fig. 4B. Azorubine concentration in dialysate of probe with 30 mm membrane, for repeated concentration changes.

Fig. 4B	Black	Green	Brown	Blue	Pink	grey
Description	Top panel: concentration increases			Bottom panel: concentration decreases		
t_0^* (min)	4.2	3.9	3.3	3.2	3.2	3.3
τ^* (min)	2.1	1.9	2.3	2.3	2.5	2.6
Mean t_0	3.8 \pm 0.4 min			3.2 \pm 0.0 min		
Mean τ	2.1 \pm 0.2 min			2.5 \pm 0.1 min		

*Standard errors of the fitted t_0 -values and τ -values are smaller than 0.1 min.

Table S4: Fitted values of Fig. 4D. Cortisol in dialysate of probe with 30 mm membrane, for repeated concentration changes. Due to limited number of datapoints, fitting was used by setting the following bounds: $2 \leq t_0 \leq 6$ and $2 \leq \tau \leq 4$. The baseline and amplitude were fixed, which were around 0 and 130-150 for the top panel (black, green, brown) and ± 130 -150 for the bottom panel (blue, pink, grey).

Fig. 4D	Black	Green	Brown	Blue	Pink	grey
Description	Top panel: concentration increases			Bottom panel: concentration decreases		
t_0 (min)	3.8 \pm 0.1	3.5 \pm 0.2	3.2 \pm 0.2	2.9 \pm 0.1	3.3 \pm 0.1	3.8 \pm 0.1
τ^* (min)	2.5	3.5 \pm 0.2	3.2 \pm 0.2	2.9 \pm 0.1	3.0	2.9 \pm 0.1
Mean t_0	3.5 \pm 0.2 min			3.3 \pm 0.4 min		
Mean τ	3.1 \pm 0.4 min			2.9 \pm 0.0 min		

*Standard errors of the fitted τ -value that are not specified are smaller than 0.1 min.

Table S5: Fitted values of Fig. 5D from left to right, top to bottom. Data was obtained for microdialysis perfused with 0.5 M NaCl in PBS and a probe with 30 mm membrane length. Cortisol concentration in dialysate is based on sampling site concentration steps from 0 to 5 μM (blue 1 and blue 2), from 5 to 20 μM (dark blue), from 20 μM to 0 (grey 1), from 5 μM to 0 (grey 2), and from 0 to 21 μM in plasma (brown). Fitting was done by using $t_0=4$ and $\tau=3$ as initial values and bounds specified as $2 \leq t_0 \leq 6$ and $2 \leq \tau \leq 4$. The initial values and bounds for y_{start} and Δy were based on the mean and median of the datapoints during the first 3 minutes and the datapoints starting at 15 minutes, respectively.

Fig. 5D	Blue 1	Dark blue	Grey 1	Blue 2	Grey 2	Brown (plasma)
Marker	Open circles	Open circles	Open circles	Filled circles	Filled circles	Open circles
Concentration step (μM)	0 to 5	5 to 20	20 to 0	0 to 5	5 to 0	0 to 21
t_0 (min)	2.9 ± 0.2	4.3	4.5	4.6	4.4	6.0
τ (min)	2.7 ± 0.3	4.0 ± 0.7	2.3 ± 0.1	4.0 ± 0.6	2.0 ± 0.1	4.0 ± 0.8

Table S6: Fitted values of Fig. S6C: Azorubine concentration in flow cell based on fluid transport with a flowrate of 100 $\mu\text{l}/\text{min}$.

Fig. S6C	Green	Blue	Brown	Pink	Grey
t_0^* (s)	39	33	35	34	32
τ^* (s)	17	24	22	21	16
Mean t_0	35 ± 2.4 s				
Mean τ	20 ± 3.0 s				

*Standard errors of the fitted t_0 -values and τ -values are smaller than 0.1 s.

Table S7: Fitted values of Fig. S7C: Azorubine concentration in dialysate (of 4 mm probe) for repeated concentration changes.

Fig. S7C	Black	Green	Brown	Blue	Pink	Grey
Description	Top panel: concentration increases			Bottom panel: concentration decreases		
t_0^* (min)	3.6	3.4	3.3	3.3	3.4	3.0
τ^* (min)	1.7	1.4	1.3	1.2	1.1	1.1
Mean t_0	3.4 ± 0.1 min			3.2 ± 0.2 min		
Mean τ	1.5 ± 0.2 min			1.1 ± 0.0 min		

* Standard errors of the fitted t_0 -values and τ -values are smaller than 0.1 min.

Table S8: Fitted values of Fig. S9E from left to right. Cortisol in dialysate (of 30 mm probe) for concentration steps from 0 to 5 μM (blue 1 and blue 2), from 5 to 20 μM (dark blue), and from 20 μM to 0 (grey 1). Fitting was done by using $t_0=4$ and $\tau=3$ as initial values and bounds specified as $2 \leq t_0 \leq 6$ and $2 \leq \tau \leq 4$. The initial values and bounds for y_{start} and Δy were based on the mean and median of the datapoints during the first 3 minutes and the datapoints starting at 15 minutes, respectively.

Fig. S9E	Blue 1	Dark blue	Grey 1	Blue 2
Marker	Open squares	Open squares	Open squares	Filled squares
Concentration step (μM)	0 to 5	5 to 20	20 to 0	0 to 5
Line type	Dashed	Dashed	Dashed	Dashed
t_0 (min)	3.8	5.5	4.3	3.4
τ (min)	2.1 ± 0.1	4.0 ± 0.2	2.2 ± 0.1	2.8 ± 0.3

11 References

- 1 V. J. A. Schuck, I. Rinas and H. Derendorf, In vitro microdialysis sampling of docetaxel, *J. Pharm. Biomed. Anal.*, 2004, **36**, 807–813.
- 2 S. Schenk, G. J. Schoenhals, G. de Souza and M. Mann, A high confidence, manually validated human blood plasma protein reference set, *BMC Med. Genomics*, 2008, **1**, 1–28.
- 3 S. Giorgi-Coll, E. P. Thelin, C. Lindblad, T. Tajsic, K. L. H. Carpenter, P. J. A. Hutchinson and A. Helmy, Dextran 500 improves recovery of inflammatory markers: An in vitro microdialysis study, *J. Neurotrauma*, 2020, **37**, 106–114.
- 4 E. G. W. M. Lentjes and F. H. T. P. M. Romijn, Temperature-dependent cortisol distribution among the blood compartments in man, *J. Clin. Endocrinol. Metab.*, 1999, **84**, 682–687.
- 5 U. B. Ottosson, B. Nilsson, R. Sodergard and B. Von Schoultz, Effects of progesterone, progestogens, and danazol on the specific cortisol binding in human plasma, *Fertil. Steril.*, 1985, **43**, 856–860.
- 6 T. G. Mayerhöfer, S. Pahlow and J. Popp, The Bouguer-Beer-Lambert Law: Shining Light on the Obscure, *Chemphyschem*, 2020, **21**, 2029–2046.
- 7 M. Taniguchi and J. S. Lindsey, Database of Absorption and Fluorescence Spectra of >300 Common Compounds for use in PhotochemCAD, *Photochem. Photobiol.*, 2018, **94**, 290–327.
- 8 D. Li, Q. Xu, Y. Liu, R. Wang, K. Xu and H. Yu, A high-accuracy measurement method of glucose concentration in interstitial fluid based on microdialysis, *Meas. Sci. Technol.*, 2017, **28**, 1–9.
- 9 A. D. Buskermolen, Y. T. Lin, L. van Smeden, R. B. van Haaften, J. Yan, K. Sergelen, A. M. de Jong and M. W. J. Prins, Continuous biomarker monitoring with single molecule resolution by measuring free particle motion, *Nat. Commun.*, 2022, **13**, 1–12.
- 10 M. H. Bergkamp, S. Cajigas, L. J. IJzendoorn and M. W. J. Prins, High-throughput single-molecule sensors: how can the signals be analyzed in real time for achieving real-time continuous biosensing, *ACS Sensors*, 2023, **8**, 2271–2281.
- 11 L. Van Smeden, A. Saris, K. Sergelen, A. M. De Jong, J. Yan and M. W. J. Prins, Reversible Immunosensor for the Continuous Monitoring of Cortisol in Blood Plasma Sampled with Microdialysis, *ACS Sensors*, 2022, **7**, 3041–3048.